Journal of Computational Physics **168,** 227–248 (2001)
doi:10.1006/jcph.2001.6696, available online at http://www.idealibrary.com on IDEAL®

A New Interface Method for Hyperbolic Problems with Discontinuous Coefficients: One-Dimensional Acoustic Example

Joël Piraux and Bruno Lombard

Laboratoire de Mécanique et d'Acoustique, 31 chemin Joseph Aiguier, 13402 Marseille Cedex 20, France
E-mail: piraux@lma.cnrs-mrs.fr

Received June 24, 1999; revised June 14, 2000

A new numerical method, called the explicit simplified interface method (ESIM), is developed in the context of acoustic wave propagation in heterogeneous media. Equations of acoustics are written as a first-order linear hyperbolic system. Apart from interfaces, a standard scheme (Lax–Wendroff, TVD, and WENO) is used in a classical way. Near interfaces, the same scheme is used, but it is applied on a set of modified values deduced from numerical values and jump conditions at interfaces. It amounts to modifying the scheme so that its order of accuracy is maintained at irregular points, despite the nonsmoothness of the solution. This easy-to-implement interface method requires only a few additional computational resources, and it can be applied to other partial differential equations.

Key Words: acoustics; heterogeneous media; Lax–Wendroff, TVD, and WENO schemes; interface methods; discontinuous coefficients.

1. INTRODUCTION

The propagation of acoustic waves in a one-space-dimension heterogeneous perfect fluid medium is considered. The density and the sound velocity are piecewise constant. The acoustic velocity u and the acoustic pressure p are computed on a uniform grid, even if interfaces do not coincide with grid points. The goal of this presentation is to develop an accurate method for the computation of u and p near interfaces, where they are not smooth.

Even if the one-dimensional problem is academic, it has some interesting applications. It is often used as a simple model in seismology or ocean acoustics, in which the ocean bottom is described as a multilayered fluid medium [1]. For the sake of simplicity, discontinuities between sediment layers can depend only on the depth below the sea floor. Furthermore, the

0021-9991/01 $35.00

description of a multilayered medium possibly involving hundreds of interfaces is useful for modeling sound propagation in a fluid medium with many inclusions or bubbles.

Equations of acoustics are usually written as a second-order scalar wave-equation for u or p. It is however useful to compute u and p simultaneously by considering the first-order hyperbolic system

$$U_t + A(x)\, U_x = 0, \tag{1}$$

where components of $U(x, t)$ are u and p, and $A(x)$ is a matrix involving physical parameters.

Many schemes can be used for the resolution of (1). A general introduction can be found in LeVeque's book [10]. Three schemes of increasing precision are used in this paper: Lax–Wendroff, TVD, and WENO. They use values of the density and of the sound speed on discrete points or averaged values of these coefficients on grid cells. As a consequence, they do not describe accurately the position and the shape (in two or three space dimensions) of interfaces cutting grid cells. Furthermore, u and p are not smooth across interfaces: it results in a loss of precision, increasing with the number of interfaces and with contrasts.

It is then interesting to use an *interface method*, such as the immersed interface method (IIM) [2, 12, 15], or the explicit jump immersed interface method (EJIIM) [14]. These numerical methods ensure a given accuracy at grid points near interfaces, but they are difficult to implement with high-order schemes, and they introduce some numerical artefacts in various cases.

A new approach called the explicit simplified interface method (ESIM) is proposed. The same scheme is used everywhere, but some values involved in time-marching near interfaces are modified. These *modified values* are deduced from numerical values of U at grid points near the interface and from jump conditions, so that the loss of accuracy because of the presence of interfaces is avoided.

The main goal of this one-dimensional study is to illustrate clearly ideas underlying the ESIM. Similar ideas can be used for other partial differential equations, such as electromagnetic or fluid mechanic ones. The paper is divided as follows. In Section 2, conservation laws, jump conditions, and some numerical schemes are recalled. In the same section, advantages and drawbacks of interface methods such as the IIM and the EJIIM are developed. The ESIM is presented in Section 3. Section 4 consists of numerical experiments including a 2D example. Section 5 concludes the paper by recalling the three key-stages of the method.

2. NUMERICAL SCHEMES AND INTERFACE METHODS

2.1. *One-Dimensional Acoustic Equations*

Conservation laws. The linearization of mechanic equations in an ideal fluid leads to

$$\begin{aligned} \rho u_t + p_x &= 0 \\ p_t + \rho c^2 u_x &= 0, \end{aligned} \tag{2}$$

where $u(x, t)$ is the acoustic velocity and $p(x, t)$ is the acoustic pressure. The density is $\rho(x)$ and the sound speed is $c(x)$. Setting

$$U(x, t) = \begin{pmatrix} u \\ p \end{pmatrix}, \quad A(x) = \begin{pmatrix} 0 & \frac{1}{\rho} \\ \rho c^2 & 0 \end{pmatrix}, \tag{3}$$

a first-order linear hyperbolic system is obtained,

$$U_t + A(x)\,U_x = 0. \tag{4}$$

Jump conditions. The location of abrupt changes in ρ and/or c is called an *interface*. Unlike gas dynamics problems, interfaces do not move. In one, two and three space dimensions, an interface is respectively a point, a curve, and a surface. This definition can be extended to boundary-value problems or singular sources [12, 14]. To keep it simple, only one interface at $x = \alpha$ is considered in Sections 2 and 3. Physical parameters are piecewise constant,

$$(\rho, c) = \begin{cases} (\rho^-, c^-) & \text{if } x \le \alpha \\ (\rho^+, c^+) & \text{if } x > \alpha. \end{cases} \tag{5}$$

It leads to constant matrices A^- if $x \le \alpha$ and A^+ otherwise:

$$A^- = \begin{pmatrix} 0 & \frac{1}{\rho^-} \\ \rho^-(c^-)^2 & 0 \end{pmatrix}, \quad A^+ = \begin{pmatrix} 0 & \frac{1}{\rho^+} \\ \rho^+(c^+)^2 & 0 \end{pmatrix}. \tag{6}$$

Writing for any function $f(x,t)$,

$$[f] = \lim_{x\to\alpha^+} f(x,t) - \lim_{x\to\alpha^-} f(x,t), \tag{7}$$

we obtain acoustic jump conditions $[u] = 0$, $[p] = 0$. It follows that

$$[U] = 0. \tag{8}$$

Jump conditions of spatial derivatives of U are deduced from (4) and (8). By induction, we can easily verify that, on both sides of α, we get

$$\begin{aligned} \frac{\partial^{2k}}{\partial t^{2k}} U &= c^{2k} \frac{\partial^{2k}}{\partial x^{2k}} U \\ \frac{\partial^{2k+1}}{\partial t^{2k+1}} U &= -c^{2k} A \frac{\partial^{2k+1}}{\partial x^{2k+1}} U, \end{aligned} \tag{9}$$

for all $k \ge 0$.

The relation (8) is true for all t. Differentiating (8) with respect to t, exchanging the order of spatial jumps and time derivatives, and using (9) leads to jump condition of any order. Setting

$$D_{2k} = \left(\frac{c^-}{c^+}\right)^{2k} I_2, \quad D_{2k+1} = \operatorname{diag}\left(\frac{\rho^-}{\rho^+}\left(\frac{c^-}{c^+}\right)^{2k+2}, \frac{\rho^+}{\rho^-}\left(\frac{c^-}{c^+}\right)^{2k}\right), \tag{10}$$

where I_2 is the 2-by-2 matrix identity, jump conditions are for all $k \ge 0$

$$\begin{aligned} \lim_{x\to\alpha^+} \frac{\partial^{2k}}{\partial x^{2k}} U(x,t) &= D_{2k} \lim_{x\to\alpha^-} \frac{\partial^{2k}}{\partial x^{2k}} U(x,t), \\ \lim_{x\to\alpha^+} \frac{\partial^{2k+1}}{\partial x^{2k+1}} U(x,t) &= D_{2k+1} \lim_{x\to\alpha^-} \frac{\partial^{2k+1}}{\partial x^{2k+1}} U(x,t). \end{aligned} \tag{11}$$

2.2. *Numerical Schemes*

Given a uniform grid with time step Δt and spatial mesh size Δx, we look to an approximation U_j^n of $U(x_j, t_n)$ at the point $(x_j = j\,\Delta x, t_n = n\,\Delta t)$, called afterwards *numerical value*. Two-level explicit finite-difference schemes are used here. They are $(2k+1)$-point spatially centered schemes, where k is called the *width* of the scheme, and time-marching is performed in two or more stages. They follow the CFL condition of stability

$$\text{CFL} = \max c\left(\frac{\Delta t}{\Delta x}\right) \leq 1. \tag{12}$$

To keep it simple, a given scheme is referred to as $\mathcal{S}$. Time-marching of a two-stage scheme $\mathcal{S}$ is written abstractly at x_j

$$U_j^{n+1} = U_j^n + \mathcal{H}\big(U_{j-k}^n, \ldots, U_{j+k}^n\big), \tag{13}$$

where the discrete operator $\mathcal{H} : R^{2\times(2k+1)} \to R^2$ is continuous [7]. Among two-stage schemes, we distinguish the 3-point Lax–Wendroff scheme ($k = 1$) and 5-point TVD schemes ($k = 2$). The Lax–Wendroff scheme is easy to implement and requires a few computational resources but it suffers from numerical dispersion (see Fig. 3b). High-order TVD schemes, based on the use of nonlinear flux limiters, allow the reduction of the spurious oscillations [10] but flatten the crests of waves (see Fig. 3c). The MC-limiter is used in Section 4 [9]. Both schemes are second-order accurate in smooth regions.

A better quality is obtained with multistage schemes such as essential non-oscillatory (ENO) schemes and WENO (weighted ENO) schemes [4, 10]. They are based on distinct discretizations of spatial and time derivatives of (4). We have implemented a spatial interpolation on three points, called WENO 5 ($k = 3$), which is fifth-order accurate in smooth regions [8]. It involves some regularity parameters $\epsilon = 10^{-6}$ and $p = 2$ (p has obviously nothing to do with the pressure). The time discretization is implemented by a fourth-order Runge–Kutta method.

The interface lies between two grid points: $x_J \leq \alpha < x_{J+1}$, as shown in Fig. 1. A point x_i is called *irregular* if time-marching at x_i uses one or more numerical value on the other side of the interface. Otherwise, a point is called *regular*. For spatially centered $(2k+1)$-point schemes used here, the set of irregular points is $\{x_{J-k+1}, \ldots, x_{J+k}\}$.

2.3. *Interface Methods*

Presentation. In one space dimension, u and p are in $\mathcal{C}^0$ across interfaces (11). In two space dimensions, the acoustic velocity component tangential to the interface is discontinuous across the interface; the acoustic pressure and the normal acoustic velocity component are in $\mathcal{C}^0$. Thus the numerical resolution of (4) with interfaces requires schemes specially designed for the computation of nonsmooth solutions. Schemes based on naive

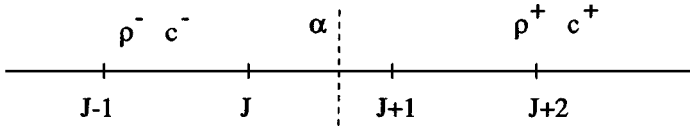

FIG. 1. 1D interface.

finite-difference approximations may give poor results. For example, the Lax–Wendroff scheme results from replacing spatial derivatives U_x and U_{xx} by centered finite-difference evaluations. This is valid only if $U(x,t)$ is smooth in the interval $[x-\Delta x, x+\Delta x]$. This is not the case at irregular points x_J and x_{J+1}, leading to a loss of accuracy.

Even with schemes especially designed for the computation of discontinuous solutions, as TVD or WENO schemes [5, 6, 11], the numerical solution suffers from a loss of accuracy when interfaces cut through grid cells [15]. This loss of accuracy is due to two reasons. Firstly, schemes do not describe accurately the position (and the shape, in two or three spaces dimensions) of interfaces. Secondly, the spatial order of accuracy is always reduced at irregular points, because of the nonsmoothness of the solution.

Moreover, schemes do not take into account jump conditions at interfaces. Therefore, the study of original jump conditions problems (such as the propagation of elastic waves across imperfect bonded media [13], or advection problems such as those defined in Chapter 2 of [15]) is difficult. Lastly, numerical instabilities can appear for high contrasts in material properties.

Schemes must be modified at irregular points in order to eliminate those problems. The resulting scheme is called an *interface method*, because it is based on jump conditions of U at the interface. Two interface methods are concisely presented in the following sections.

The immersed interface method (IIM). One way is to write explicitly a new scheme at irregular points: this is the aim of the Immersed Interface Method (IIM). The method was developed by Li and LeVeque [12], extended to acoustics and elasticity by Zhang [15, 16], and to Navier–Stokes by Calhoun [2]. In [15], the Lax–Wendroff scheme is used at regular points. A new 3-point finite-difference scheme is written at irregular points,

$$\begin{aligned} U_J^{n+1} &= U_J^n + \frac{\Delta t}{\Delta x}\left(\Gamma_{J,1}\,U_{J-1}^n + \Gamma_{J,2}\,U_J^n + \Gamma_{J,3}\,U_{J+1}^n\right) \\ U_{J+1}^n &= U_{J+1}^n + \frac{\Delta t}{\Delta x}\left(\Gamma_{J+1,1}\,U_{J+2}^n + \Gamma_{J+1,2}\,U_{J+1}^n + \Gamma_{J+1,3}\,U_J^n\right). \end{aligned} \tag{14}$$

The Γ's are 2-by-2 matrices, defined so that (14) is a second-order accurate approximation of (4) at x_J and x_{J+1}. The analysis of local truncation error at x_J and x_{J+1} leads to a system of matrix equations whose solutions are Γ's, computed only one time during a preprocessing stage. At each time step, only some matrix–vector multiplications (14) need to be done at irregular points, which is very low-cost. The IIM can be coupled with other schemes: Zhang has demonstrated that numerical solutions are improved when a TVD scheme is used in conjunction with the second-order IIM (4). Using limiter functions reduces the order of accuracy but helps to dampen oscillations and to reduce phase errors. The IIM can be developed also to higher orders for coupling with high-order schemes (such as WENO 5).

However, the use of the IIM has some drawbacks. For identical material properties on both sides of α, special formula (14) recover the original Lax–Wendroff scheme; even in the general case of distinct material properties, the second-order IIM is dispersive. So, if formula (14) are used at irregular points and coupled with a TVD scheme (that is not dispersive), numerical dispersion is introduced at two points per interface: for a high number of interfaces, it introduces a large amount of numerical artefacts. In a general manner, building an IIM that mimics the properties of the scheme $\mathcal{S}$—for example ensuring TVD properties in the case of a TVD scheme, or minimizing oscillations in the case of the WENO

5 scheme—can become very complicated. Moreover, in the case of TVD scheme ($k = 2$), limiters introduce two additional irregular points, x_{J-1} and x_{J+2}, where no interface method is used.

The explicit jump immersed interface method (EJIIM). A modification and extension of the IIM has been developed by Wiegmann and Bube [14] in the context of elliptic equations, called the explicit jump immersed interface method (EJIIM). Corrections are added to the chosen scheme at irregular points, so that the local truncation error is maintained. In the limit case of identical material properties, corrections are equal to zero, recovering the original scheme. However, it is again difficult to calculate corrections in the case of a complicated scheme $\mathcal{S}$. Moreover, corrections are deduced from one-sided interpolations of U. When coupling the EJIIM and the Lax–Wendroff scheme, we have observed instabilities even for moderate contrasts. We suppose that they come from these nonsymmetrical interpolations.

3. THE EXPLICIT SIMPLIFIED INTERFACE METHOD (ESIM)

3.1. *Introduction*

In the previous section, we stressed some properties, constraints, and remarks about interface methods, summed up as follows:

- The order of accuracy of the scheme $\mathcal{S}$ must be maintained at all irregular points, whatever the position of the interface;
- We do not want to write explicitly a new scheme (like the IIM) or corrections depending on $\mathcal{S}$ (like the EJIIM);
- The scheme $\mathcal{S}$ must be recovered in the limit case of identical material properties on both sides of α (like the EJIIM);
- Interpolations used by the interface method must be two-sided and symmetrical in relation to α, in order to avoid instabilities.

Therefore, we propose a new method called the explicit simplified interface method (ESIM). Its design wants to achieve the four previous remarks. For the rest of the section, we will mainly consider a two-stage scheme $\mathcal{S}$.

Modified solutions and modified values. The first part of the method consists in building, on each side of α and at time $t = t_n$, a smooth extension $U^*(x, t_n)$ of the exact solution $U(x, t_n)$ on the other side. These extensions are called *modified solutions*. This is schematized in Fig. 2 in the case of a scalar discontinuous function $U(x, t_n)$ (solid line): this is not the acoustic case (u and p are continuous), but it is more clear. Modified solutions $U^*(x, t_n)$ are drawn in dotted lines and are defined so that functions

$$\tilde{U}_1(x, t_n) = \begin{cases} U(x, t_n) & \text{if } x_{J-2k+1} \le x < \alpha \\ U^*(x, t_n) & \text{if } \alpha \le x \le x_{J+k} \end{cases},$$
$$\tilde{U}_2(x, t_n) = \begin{cases} U^*(x, t_n) & \text{if } x_{J-k+1} \le x \le \alpha \\ U(x, t_n) & \text{if } \alpha < x \le x_{J+2k} \end{cases} \tag{15}$$

are smooth up to an arbitrary order. Recall that k is the width of the scheme $\mathcal{S}$: so, $\tilde{U}_1(x, t_n)$ and $\tilde{U}_2(x, t_n)$ are defined on the range of values used for time-marching respectively at

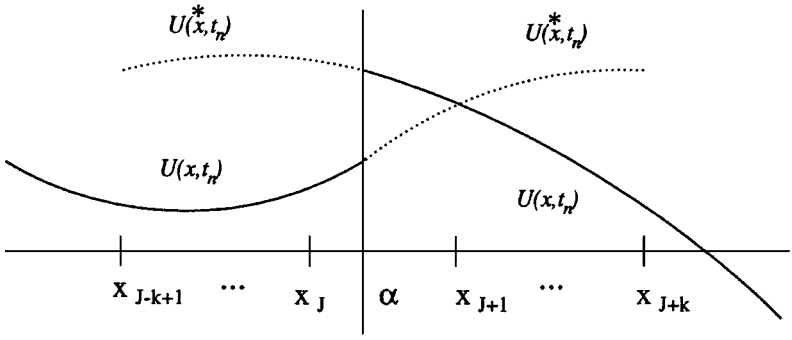

FIG. 2. Exact solution $U(x, t_n)$ (-) and modified solutions $U^*(x, t_n)$ $(\cdots)$.

left-sided and at right-sided irregular points. Let us examine the first function $\tilde{U}_1(x, t_n)$ and the modified solution $U^*(x, t_n)$ on the right (15). We impose the conditions

$$m = 0, \ldots, 2p-1, \quad \frac{\partial^m}{\partial x^m} U^*(\alpha, t_n) = \frac{\partial^m}{\partial x^m} U(\alpha^-, t_n), \tag{16}$$

so that $\tilde{U}_1$ is in $\mathcal{C}^{2p-1}$ on $[x_{J-2k+1}, x_{J+k}]$. The integer p is discussed further (p has obviously nothing to do here with the acoustic pressure). The condition (16) is valid only for a sufficiently smooth initial value $U_0(x) = U(x, 0)$: for $U_0(x)$ in $\mathcal{C}^s$, the exact solution $U(x, t)$ is in $\mathcal{C}^s$ on the left side ($x < \alpha$) and on the right side ($x > \alpha$). Limit values $\frac{\partial^m}{\partial x^m} U(\alpha^-, t_n)$ can be defined up to $m = s$, and (16) is well-defined under the condition $2p - 1 \leq s$. One way to ensure (16) is to write the modified solution on the right $U^*(x, t_n)$ as a polynomial,

$$U^*(x, t_n) = \sum_{m=0}^{2p-1} \frac{(x-\alpha)^m}{m!} \frac{\partial^m}{\partial x^m} U(\alpha^-, t_n). \tag{17}$$

In fact, we can only obtain estimations of limit values $\frac{\partial^m}{\partial x^m} U(\alpha^-, t_n)$. Therefore, only estimations of $U^*(x, t_n)$ and $\tilde{U}_1(x, t_n)$, based on numerical values, can be found. Actually, these estimations will be avoided: *modified values* (i.e., values at right-sided irregular points of the estimation of $U^*(x, t_n)$) are determined directly and explicitly from numerical values. A similar discussion holds for $U^*(x, t_n)$ and modified values on the left, with limit values $\frac{\partial^m}{\partial x^m} U(\alpha^+, t_n)$.

Using modified values. The second part of the method consists of using the scheme $\mathcal{S}$ everywhere, but some modified values are used for time-marching at irregular points. Suppose that x_i is an irregular point. The key idea is to apply at x_i the scheme $\mathcal{S}$ on values of the smooth function $\tilde{U}_1(x, t_n)$ if $x_i \leq \alpha$ (resp. $\tilde{U}_2(x, t_n)$ if $x_i > \alpha$). Thus the scheme $\mathcal{S}$ uses at x_i *numerical values* at points on the same side of the interface as x_i (as usually), and *modified values* at points on the other side of the interface. Remarks of the beginning of the section have been taken into account in the following way:

- From a minimal number of numerical values U_l^n's used for the determination of modified values U_j^*'s, the order of the couplage "scheme $\mathcal{S}$ + ESIM" at irregular points is the same as the order of the scheme $\mathcal{S}$ at regular points. See Section 3.4 for the demonstration.
- Unlike the IIM or the EJIIM, the scheme $\mathcal{S}$ is modified implicitly. All the difficulty of the method is transferred on the determination of modified values (see Section 3.2), which

is explicit and very easy (see (25) and (29)). Coupling WENO 5 with the ESIM is not harder than coupling Lax–Wendroff with the ESIM. It justifies the name "simplified."

- In the borderline case where material properties are the same on both sides of α, $U_i^n = U_i^*$ at all irregular points (see Section 3.3). Then, the scheme $\mathcal{S}$ in homogeneous medium is completely recovered.
- Determinations of modified values are symmetrical in relation to α. The stability is discussed qualitatively in Section 3.6.

3.2. *Construction of Modified Values*

Construction of modified values on the right. Limit values $\frac{\partial^m}{\partial x^m} U(\alpha^-, t_n)$ required for $U^*(x, t_n)$ (17) are now estimated. Taylor series expansions of $2p$-th order are written around α

$$i = J - p + 1, \ldots, J + p, \quad U(x_i, t_n) = \sum_{m=0}^{2p-1} \frac{(x_i - \alpha)^m}{m!} \frac{\partial^m}{\partial x^m} U(\alpha^{\pm}, t_n) + O(\Delta x^{2p}), \quad (18)$$

where $\alpha^{\pm}$ refers to α^- if $x < \alpha$ and to α^+ otherwise. The notation $O(\Delta x^{\lambda})$, generally used for a scalar, refers here to a vector of an arbitrary size (depending on the context) whose entries are $O(\Delta x^{\lambda})$ scalars. From jump conditions (11), we get

$$m = 0, \ldots, 2p - 1, \quad \frac{\partial^m}{\partial x^m} U(\alpha^+, t_n) = D_m \frac{\partial^m}{\partial x^m} U(\alpha^-, t_n). \quad (19)$$

According to the position of x_i, Eq. (18) are

$$\begin{aligned} i &= J - p + 1, \ldots, J, \quad U(x_i, t_n) = \sum_{m=0}^{2p-1} \frac{(x_i - \alpha)^m}{m!} \frac{\partial^m}{\partial x^m} U(\alpha^-, t_n) + O(\Delta x^{2p}) \\ i &= J + 1, \ldots, J + p, \quad U(x_i, t_n) = \sum_{m=0}^{2p-1} \frac{(x_i - \alpha)^m}{m!} D_m \frac{\partial^m}{\partial x^m} U(\alpha^-, t_n) + O(\Delta x^{2p}). \end{aligned} \quad (20)$$

Equations (20) are written using a matrix formulation, as

$$\begin{pmatrix} U(x_{J-p+1}, t_n) \\ \vdots \\ U(x_{J+p}, t_n) \end{pmatrix} = \mathcal{M}_{p,p} \begin{pmatrix} U(\alpha^-, t_n) \\ \vdots \\ \frac{\partial^{2p-1}}{\partial x^{2p-1}} U(\alpha^-, t_n) \end{pmatrix} + O(\Delta x^{2p}), \quad (21)$$

where $\mathcal{M}_{p,q}$ is defined as a $(2p)$-by-$(2q)$ block matrix with 2-by-2 blocks ($n = 1, \ldots, 2q$):

$$\mathcal{M}_{p,q}[m, n] = \begin{cases} \frac{(x_{J-p+m} - \alpha)^{n-1}}{(n-1)!} I_2 & \text{if } m \in [1, p] \\ \frac{(x_{J-p+m} - \alpha)^{n-1}}{(n-1)!} D_{n-1} & \text{if } m \in [p+1, 2p]. \end{cases} \quad (22)$$

Even if $q = p$ in (21), the general definition of $\mathcal{M}_{p,q}$ (22) is useful in Section 3.6. Limit values $\frac{\partial^m}{\partial x^m} U(\alpha^-, t_n)$ could be obtained by inverting (21), leading to $U^*(x, t_n)$ and $\tilde{U}_1(x, t_n)$. However, exact values and truncation errors are unknown. Exact values $U(x_i, t_n)$ are then replaced in (21) by numerical values U_i^n and the vector of truncation errors is eliminated. Limit

values $\frac{\partial^m}{\partial x^m} U(\alpha^-, t_n)$ are replaced by numerical estimations: for the sake of simplicity, these estimations are written $\frac{\partial^m}{\partial x^m} U_1^-$. The subscript indicates that they are used for the construction of $\tilde{U}_1$, the operator $\frac{\partial^m}{\partial x^m}$ is only symbolic, and the superscript refers to α^-. Then we write

$$\begin{pmatrix} U^n_{J-p+1} \\ \vdots \\ U^n_{J+p} \end{pmatrix} = \mathcal{M}_{p,p} \begin{pmatrix} U_1^- \\ \vdots \\ \frac{\partial^{2p-1}}{\partial x^{2p-1}} U_1^- \end{pmatrix}. \tag{23}$$

Estimations of the limit values are obtained by inverting (23). This leads to an estimation of the modified solution (17) and to modified values,

$$i = J+1, \ldots, J+k, \quad U_i^* = \sum_{m=0}^{2p-1} \frac{(x_i - \alpha)^m}{m!} \frac{\partial^m}{\partial x^m} U_1^-. \tag{24}$$

Using (23), we obtain explicitly U_i^*'s on the right

$$i = J+1, \ldots, J+k, \quad U_i^* = \left(1, \ldots, \frac{(x_i - \alpha)^{2p-1}}{(2p-1)!}\right) \mathcal{M}^{-1}_{p,p} \begin{pmatrix} U^n_{J-p+1} \\ \vdots \\ U^n_{J+p} \end{pmatrix}. \tag{25}$$

Construction of modified values on the left. The same method is used to define $\tilde{U}_2(x, t_n)$ and to compute modified values on the left. The expression $\frac{\partial^m}{\partial x^m} U_2^+$ refers to a numerical estimation of $\frac{\partial^m}{\partial x^m} U(\alpha^+, t_n)$. We write

$$\begin{pmatrix} U^n_{J-p+1} \\ \vdots \\ U^n_{J+p} \end{pmatrix} = \mathcal{N}_{p,p} \begin{pmatrix} U_2^+ \\ \vdots \\ \frac{\partial^{2p-1}}{\partial x^{2p-1}} U_2^+ \end{pmatrix}, \tag{26}$$

where $\mathcal{N}_{p,q}$ is a $(2p)$-by-$(2q)$ block matrix with 2-by-2 blocks ($n = 1, \ldots, 2q$):

$$\mathcal{N}_{p,q}[m,n] = \begin{cases} \frac{(x_{J-p+m} - \alpha)^{n-1}}{(n-1)!} D_{n-1}^{-1} & \text{if } m \in [1, p] \\ \frac{(x_{J-p+m} - \alpha)^{n-1}}{(n-1)!} I_2 & \text{if } m \in [p+1, 2p]. \end{cases} \tag{27}$$

Modified values on the left are

$$i = J-k+1, \ldots, J, \quad U_i^* = \sum_{m=0}^{2p-1} \frac{(x_i - \alpha)^m}{m!} \frac{\partial^m}{\partial x^m} U_2^+. \tag{28}$$

Using (26), U_i^*'s on the left are obtained explicitly

$$i = J-k+1, \ldots, J, \quad U_i^* = \left(1, \ldots, \frac{(x_i - \alpha)^{2p-1}}{(2p-1)!}\right) \mathcal{N}^{-1}_{p,p} \begin{pmatrix} U^n_{J-p+1} \\ \vdots \\ U^n_{J+p} \end{pmatrix}. \tag{29}$$

3.3. *Using Modified Values: ESIM p-p*

At an irregular point x_j, time-marching of a two-stage scheme $\mathcal{S}$ uses modified values at points on the other side of α as x_j. It is written abstractly (cf (13)) as

$$\begin{aligned} &J-k+1 \le j \le J, \quad U_j^{n+1} = U_j^n + \mathcal{H}\big(U_{j-k}^n, \ldots, U_J^n,\ U_{J+1}^*, \ldots, U_{j+k}^*\big) \\ &J+1 \le j \le J+k, \quad U_j^{n+1} = U_j^n + \mathcal{H}\big(U_{j-k}^*, \ldots, U_J^*,\ U_{J+1}^n, \ldots, U_{j+k}^n\big). \end{aligned} \tag{30}$$

This method is referred to as ESIM p-p. The application of ESIM to multistage schemes such as WENO 5 is obvious. The construction of modified values at one stage uses numerical values at the previous stage. For the couplage "WENO 5 + ESIM p-p," the procedure is repeated four times during a time step (i.e., at each Runge–Kutta integration).

Matrices $\mathcal{M}_{p,p}^{-1}$ and $\mathcal{N}_{p,p}^{-1}$ (Eqs. (25) and (29)) are computed explicitly only one time, during a preprocessing step. At each time step, only matrix–vector multiplications (Eqs. (25) and (29)) need to be done. The computational cost is very low. We can show that $\mathcal{M}_{p,p}$ and $\mathcal{N}_{p,p}$ can be inverted—whatever the position of the interface and the values of physical parameters—by calculating their determinant. For example, let us see the case of $\mathcal{M}_{1,1}$. Setting

$$\epsilon = \frac{\alpha - J\Delta x}{\Delta x}, \tag{31}$$

we get

$$\det \mathcal{M}_{1,1} = \left[(1-\epsilon)\frac{\rho^-}{\rho^+}\left(\frac{c^-}{c^+}\right)^2 + \epsilon\right]\left[(1-\epsilon)\frac{\rho^+}{\rho^-} + \epsilon\right]\Delta x^2, \tag{32}$$

which is always different from zero for positive values of $\rho^\pm$ and $c^\pm$, and for $0 \le \epsilon < 1$. It has been verified also for $\mathcal{M}_{p,p}$ and $\mathcal{N}_{p,p}$, up to $p = 3$.

For identical properties on both sides of α, $D_m = I_2$ (10). For a right-sided irregular point x_i, we deduce from (22), (23), and (24) that

$$i = J+1, \ldots, J+k, \quad U_i^* = U_i^n, \tag{33}$$

if $k \le p$. A similar property holds for left-sided irregular points. Therefore, the scheme $\mathcal{S}$ in homogeneous medium is completely recovered under the condition $k \le p$.

3.4. *Local Truncation Error Analysis*

Let x_j be a left-sided irregular point ($x_j \le \alpha$). For a given two-stage scheme $\mathcal{S}$, we seek the local truncation error $\mathcal{L}_1(x_j, t_n)$ of the couplage "scheme $\mathcal{S}$ + ESIM p-p" at x_j. First, $\mathcal{L}_1(x_j, t_n)$ is developed. Second, an auxiliary problem is defined, whose solution and local truncation error $\mathcal{L}_2(x_j, t_n)$ are known. Comparing $\mathcal{L}_2(x_j, t_n)$ and $\mathcal{L}_1(x_j, t_n)$ leads to an explicit value of $\mathcal{L}_1(x_j, t_n)$.

Couplage "scheme $\mathcal{S}$ + ESIM p-p". Time-marching at x_j is based on modified values (30), leading to

$$\frac{1}{\Delta t}\left(U_j^{n+1} - U_j^n\right) - \frac{1}{\Delta t}\mathcal{H}\left(U_{j-k}^n, \ldots, U_J^n,\ U_{J+1}^*, \ldots, U_{j+k}^*\right) = 0. \tag{34}$$

To get the local truncation error $\mathcal{L}_1(x_j, t_n)$, we replace each numerical value that appears explicitly or implicitly in (34) by its exact value. The structure of (34) leads to $\mathcal{L}_1(x_j, t_n)$ as the difference of two quantities $\mathcal{L}_1^1(x_j, t_n)$ and $\mathcal{L}_1^2(x_j, t_n)$. The first part $\mathcal{L}_1^1(x_j, t_n)$ is obtained from Taylor series expansions of $U(x_j, t_{n+1})$ at t_n,

$$\begin{aligned}\mathcal{L}_1^1(x_j, t_n) &= \frac{1}{\Delta t}[U(x_j, t_{n+1}) - U(x_j, t_n)] \\ &= \sum_{m=1}^{2p-1} \frac{\Delta t^{m-1}}{m!} \frac{\partial^m}{\partial t^m} U(x_j, t_n) + O(\Delta x^{2p-1}). \end{aligned} \tag{35}$$

Recall that Δt and Δx are linked by the CFL number (12): $O(\Delta t^\lambda) = O(\Delta x^\lambda)$ for all λ. For the second part $\mathcal{L}_1^2(x_j, t_n)$ of $\mathcal{L}_1(x_j, t_n)$, Taylor series are written at α^- on the left side ($i = j - k + 1, \ldots, J$),

$$U(x_i, t_n) = \sum_{m=0}^{2p-1} \frac{(x_i - \alpha)^m}{m!} \frac{\partial^m}{\partial x^m} U(\alpha^-, t_n) + O(\Delta x^{2p}). \tag{36}$$

On the right side ($i = J + 1, \ldots, J + k$), modified values U_i^*'s are replaced by $\mathcal{U}^*(x_i, t_n)$ (25),

$$\mathcal{U}^*(x_i, t_n) = \left(1, \ldots, \frac{(x_i - \alpha)^{2p-1}}{(2p-1)!}\right) \mathcal{M}_{p,p}^{-1} \begin{pmatrix} U(x_{J-p+1}, t_n) \\ \vdots \\ U(x_{J+p}, t_n) \end{pmatrix}. \tag{37}$$

From (21), we get

$$\begin{aligned}\mathcal{U}^*(x_i, t_n) &= \left(1, \ldots, \frac{(x_i - \alpha)^{2p-1}}{(2p-1)!}\right) \mathcal{M}_{p,p}^{-1} \left[\mathcal{M}_{p,p} \begin{pmatrix} U(\alpha^-, t_n) \\ \vdots \\ \frac{\partial^{2p-1}}{\partial x^{2p-1}} U(\alpha^-, t_n) \end{pmatrix} + O(\Delta x^{2p}) \right] \\ &= \sum_{m=0}^{2p-1} \frac{(x_i - \alpha)^m}{m!} \frac{\partial^m}{\partial x^m} U(\alpha^-, t_n) + O(\Delta x^{2p}). \end{aligned} \tag{38}$$

The estimation of the error in (38) is based on two results. First, we can determine the order of magnitude for the entries in the block vector,

$$\tau = \mathcal{M}_{p,p}^{-1} O(\Delta x^{2p}) = {}^t(O(\Delta x^{2p}), \ldots, O(\Delta x)). \tag{39}$$

A similar result is shown in [2]. Second, we have obviously

$$\left(1, \ldots, \frac{(x_i - \alpha)^{2p-1}}{(2p-1)!}\right) \tau = O(\Delta x^{2p}). \tag{40}$$

Transferring values (36) and (38) into $\mathcal{L}_1^2(x_j, t_n)$ leads to

$$\mathcal{L}_1^2(x_j, t_n) = \frac{1}{\Delta t}\,\mathcal{H}\left(\sum_{m=0}^{2p-1} \frac{(x_{j-k}-\alpha)^m}{m!}\,\frac{\partial^m}{\partial x^m}\,U(\alpha^-, t_n) + O(\Delta x^{2p}), \ldots, \right.$$
$$\left. \sum_{m=0}^{2p-1} \frac{(x_{j+k}-\alpha)^m}{m!}\,\frac{\partial^m}{\partial x^m}\,U(\alpha^-, t_n) + O(\Delta x^{2p}) \right). \tag{41}$$

The discrete operator $\mathcal{H}$ is continuous [7]; hence

$$\mathcal{L}_1^2(x_j, t_n) = \frac{1}{\Delta t}\,\mathcal{H}\left(\sum_{m=0}^{2p-1} \frac{(x_{j-k}-\alpha)^m}{m!}\,\frac{\partial^m}{\partial x^m}\,U(\alpha^-, t_n), \ldots, \right.$$
$$\left. \sum_{m=0}^{2p-1} \frac{(x_{j+k}-\alpha)^m}{m!}\,\frac{\partial^m}{\partial x^m}\,U(\alpha^-, t_n) \right) + O(\Delta x^{2p-1}). \tag{42}$$

We recall

$$\mathcal{L}_1(x_j, t_n) = \mathcal{L}_1^1(x_j, t_n) - \mathcal{L}_1^2(x_j, t_n). \tag{43}$$

Auxiliary problem. Let us consider the function

$$V(x, t) = \sum_{\lambda=0}^{2p-1} \frac{(x-\alpha)^\lambda}{\lambda!}\,\frac{\partial^\lambda}{\partial x^\lambda}\,U(\alpha^-, t), \tag{44}$$

where $U(x, t)$ is the solution of $U_t + A^- U_x = 0$. We can easily verify that $V(x, t)$ is smooth across α and is the solution of the Cauchy problem

$$V_t + A^-\,V_x = \frac{(x-\alpha)^{2p-1}}{(2p-1)!}\,\frac{\partial^{2p}}{\partial x^{2p}}\,U(\alpha^-, t)$$
$$V_0(x) = V(x, 0) = \sum_{\lambda=0}^{2p-1} \frac{(x-\alpha)^\lambda}{\lambda!}\,\frac{\partial^\lambda}{\partial x^\lambda}\,U(\alpha^-, 0). \tag{45}$$

A condition on $U_0(x)$, slightly more strict than $2p-1 \geq s$, is then required: limit values $\frac{\partial^{2p}}{\partial x^{2p}}\,U(\alpha^\pm, t)$ must be defined for all t. The scheme $\mathcal{S}$ is used for the resolution of (45), so that a local truncation error $\mathcal{L}_2(x_j, t_n)$ is defined. For the exact solution (44) of (45), we can develop $\mathcal{L}_2(x_j, t_n)$

$$\mathcal{L}_2(x_j, t_n) = \underbrace{\frac{V(x_j, t_{n+1}) - V(x_j, t_n)}{\Delta t}}_{\mathcal{L}_2^1(x_j, t_n)} - \underbrace{\frac{1}{\Delta t}\mathcal{H}(V(x_{j-k}, t_n), \ldots, V(x_{j+k}, t_n))}_{\mathcal{L}_2^2(x_j, t_n)}. \tag{46}$$

A Taylor expansion of $V(x_j, t_{n+1})$ is written around t_n:

$$\mathcal{L}_2^1(x_j, t_n) = \sum_{m=1}^{2p-1} \frac{\Delta t^{m-1}}{m!}\,\frac{\partial^m}{\partial t^m}\,V(x_j, t_n) + O(\Delta x^{2p-1}). \tag{47}$$

For $m = 1, \ldots, 2p-1$, (44) leads to

$$\begin{aligned}\frac{\partial^m}{\partial t^m} V(x_j, t_n) &= \frac{\partial^m}{\partial t^m}\left(\sum_{\lambda=0}^{2p-1-m} \frac{(x_j-\alpha)^\lambda}{\lambda!} \frac{\partial^\lambda}{\partial x^\lambda} U(\alpha^-, t_n) \right. \\ &\quad \left. + (x_j-\alpha)^{2p-m} \sum_{\lambda=2p-m}^{2p-1} \frac{(x_j-\alpha)^{\lambda-(2p-m)}}{\lambda!} \frac{\partial^\lambda}{\partial x^\lambda} U(\alpha^-, t_n) \right) \\ &= \frac{\partial^m}{\partial t^m}\left(\sum_{\lambda=0}^{2p-1-m} \frac{(x_j-\alpha)^\lambda}{\lambda!} \frac{\partial^\lambda}{\partial x^\lambda} U(\alpha^-, t_n) + O(\Delta x^{2p-m}) \right). \end{aligned} \tag{48}$$

Hence, we have

$$\mathcal{L}_2^1(x_j, t_n) = \sum_{m=1}^{2p-1} \frac{\Delta t^{m-1}}{m!} \frac{\partial^m}{\partial t^m}\left(\sum_{\lambda=0}^{2p-1-m} \frac{(x_j-\alpha)^\lambda}{\lambda!} \frac{\partial^\lambda}{\partial x^\lambda} U(\alpha^-, t_n) \right) + O(\Delta x^{2p-1}). \tag{49}$$

For each m, Taylor series expansions of $U(x_j, t_n)$ are written around α^-

$$\sum_{\lambda=0}^{2p-1-m} \frac{(x_j-\alpha)^\lambda}{\lambda!} \frac{\partial^\lambda}{\partial x^\lambda} U(\alpha^-, t_n) = U(x_j, t_n) + O(\Delta x^{2p-m}), \tag{50}$$

hence, we have

$$\mathcal{L}_2^1(x_j, t_n) = \sum_{m=1}^{2p-1} \frac{\Delta t^{m-1}}{m!} \frac{\partial^m}{\partial t^m} U(x_j, t_n) + O(\Delta x^{2p-1}). \tag{51}$$

For the computation of $\mathcal{L}_2^2(x_j, t_n)$, $V(x_j, t_n)$ is replaced by its exact value (44)

$$\begin{aligned}\mathcal{L}_2^2(x_j, t_n) = \frac{1}{\Delta t} \mathcal{H}\left(\sum_{m=0}^{2p-1} \frac{(x_{j-k}-\alpha)^m}{m!} \frac{\partial^m}{\partial x^m} U(\alpha^-, t_n), \ldots, \right. \\ \left. \sum_{m=0}^{2p-1} \frac{(x_{j+k}-\alpha)^m}{m!} \frac{\partial^m}{\partial x^m} U(\alpha^-, t_n) \right). \end{aligned} \tag{52}$$

We recall

$$\mathcal{L}_2(x_j, t_n) = \mathcal{L}_2^1(x_j, t_n) - \mathcal{L}_2^2(x_j, t_n). \tag{53}$$

Conclusion. From (35), (42), (51), and (52), $\mathcal{L}_1(x, j, t_n)$ and $\mathcal{L}_2(x, j, t_n)$ are compared:

$$\left.\begin{aligned}\mathcal{L}_1^1(x_j, t_n) &= \mathcal{L}_2^1(x_j, t_n) + O(\Delta x^{2p-1}) \\ \mathcal{L}_1^2(x_j, t_n) &= \mathcal{L}_2^2(x_j, t_n) + O(\Delta x^{2p-1})\end{aligned}\right\} \Rightarrow \mathcal{L}_1(x_j, t_n) = \mathcal{L}_2(x_j, t_n) + O(\Delta x^{2p-1}). \tag{54}$$

$V(x, t)$ is smooth on $[x_{j-k}, x_{j+k}]$ at each time t. Moreover, we have supposed that the scheme $\mathcal{S}$ is r-th order accurate. So, we get $\mathcal{L}_2(x_j, t_n) = O(\Delta x^r)$ [10]. Thus, the couplage "scheme $\mathcal{S}$ + ESIM p-p" is r-th order accurate under the condition

$$2p - 1 \geq r. \tag{55}$$

A similar result can be obtained for multistage schemes such as WENO 5.

3.5. *Choice of p*

We seek the smallest values of p that optimize the couplage "scheme $\mathcal{S}$ + ESIM p-p." The main constraints and results previously found are summed up as follows:

- $s \geq 2p-1$ (required for the definition of $U^*(x,t_n)$);
- $2p-1 \geq r \Rightarrow \mathcal{L}_1 = O(\Delta_x^2)$;
- $p \geq k \Rightarrow U_i^* = U_i^n$ if $\rho^- = \rho^+$ and $c^- = c^+$.

Recall that r and k are respectively the order and the width of the scheme, $\mathcal{L}_1$ is the local truncation order of the couplage "scheme $\mathcal{S}$ + ESIM p-p" at irregular points, and s is the smoothness of the initial value $U_0(x) = U(x,0)$. It leads to

$$\begin{aligned} p &= \max\left[k, r+1-E\left(\frac{r+1}{2}\right)\right] \\ s &= 2p-1, \end{aligned} \tag{56}$$

where $E(x)$ is the greatest integer less than or equal to x. For greater values of p, the precision does not increase, whereas the computational cost grows. As a consequence, Lax–Wendroff and TVD schemes are associated with ESIM 2-2, and WENO 5 is associated with ESIM 3-3. We recall that left values and right values of $\frac{\partial^{2p}}{\partial x^{2p}} U_0(x)$ must be defined everywhere.

3.6. *Stability*

Introduction. We do not propose a theory of stability for the couplage "scheme $\mathcal{S}$ + ESIM p-p." Nevertheless, we have considered this problem in detail through computations, for various positions of the interface, physical parameters, and CFL numbers.

We have never observed instabilities in the case "WENO 5 + ESIM 3-3" up to CFL = 1, even for very high contrasts (such as water–air) and for an interface very close to a grid point, or on a grid point ($\epsilon = 0$). In each case, measures of errors have shown a fifth-order convergence of the couplage (see Section 4).

The couplages "Lax–Wendroff + ESIM 2-2" and "TVD + ESIM 2-2" are stable also, except in the two limit cases

$$\begin{aligned} &\rho^- \gg \rho^+,\ c^- \gg c^+ \quad \text{and} \quad \epsilon \to 1^- \\ &\rho^- \ll \rho^+,\ c^- \ll c^+ \quad \text{and} \quad \epsilon \to 0^+. \end{aligned} \tag{57}$$

We have not obtained theoretical limit values of ϵ, $\rho^\pm$, and $c^\pm$, and it remains an interesting open question. However, we can express some remarks. First, this problem of stability also exists in the case of the IIM, with the same limit values of ϵ, $\rho^\pm$, and $c^\pm$. Second, the behavior of Lax–Wendroff and TVD schemes coupled with ESIM 2-2 are the same: instabilities appear exactly from the same limit values of ϵ, $\rho^\pm$, and $c^\pm$. Thirdly, the value of p has an influence on the stability. For example, coupling the Lax–Wendroff scheme with ESIM p-p ($p = 1, 2, 3$) in the case of water–air leads to instabilities for the following limit values of ϵ:

$$\begin{aligned} p=1:&\quad \epsilon \geq 0.99 \\ p=2:&\quad \epsilon \geq 0.999 \\ p=3:&\quad \epsilon \geq 0.9999. \end{aligned} \tag{58}$$

However, increasing p is not a satisfactory solution: it is not well-matched to second-order schemes such as Lax–Wendroff and TVD.

Least-square resolution. To solve the previous problematic cases, we propose another determination of modified values that does not produce instabilities. The process of ESIM 2-2—described in Section 3.2—involves the use of four numerical values on both sides of α and estimation of spatial derivatives of U up to third order. We propose now to estimate those four limit values with *six* numerical values of U on both sides of α. So, for the construction of modified values on the right, we write

$$\begin{pmatrix} U^n_{J-2} \\ \vdots \\ U^n_{J+3} \end{pmatrix} = \mathcal{M}_{3,2} \begin{pmatrix} U_1^- \\ \vdots \\ \frac{\partial^3}{\partial x^3} U_1^- \end{pmatrix}, \tag{59}$$

where $\mathcal{M}_{3,2}$ is the rectangular matrix (22) with $p = 3$ and $q = 2$. Equation (59) is solved by least-square, so that modified values on the right are

$$i = 1, 2, \quad U_i^* = \left(1, \ldots, \frac{(x_i - \alpha)^3}{3!}\right) ({}^t\mathcal{M}_{3,2}\,\mathcal{M}_{3,2})^{-1}\,{}^t\mathcal{M}_{3,2} \begin{pmatrix} U^n_{J-2} \\ \vdots \\ U^n_{J+3} \end{pmatrix}. \tag{60}$$

The same procedure is applied for modified values on the left; this is logically called ESIM 3-2. We have never observed instabilities in doing this procedure, whatever the physical parameters and the position of the interface. A similar least-square procedure: "Lax–Wendroff + ESIM 2-1" has been used for $\epsilon \geq 0.99$ without producing instabilities (cf (58)).

The analysis of truncation error exposed in Section 3.4 is always valid. Coupling "Lax–Wendroff + ESIM 3-2" and "TVD + ESIM 3-2" is second-order accurate as it is confirmed by measures of errors. Explaining the stability of ESIM 3-2 remains another interesting question. Furthermore, this least-squares resolution will be systematically used in 2D and 3D application of the ESIM, as will be presented in a future paper.

4. NUMERICAL RESULTS

Three numerical tests are proposed. The first one concerns the propagation of an acoustic wave across a single interface with moderate contrasts. The analysis of Section 3.4 is confirmed by measures of errors. The second test extends the previous study to very large contrasts. The last example introduces a future study of the ESIM in 2D and 3D. A study of the computational cost is not provided here, because it is almost negligible in the one-dimensional case.

4.1. *A Single Interface*

The simple acoustic problem of a single interface ($\alpha = 96.3$ m) is considered, with a 300 m long fluid medium and physical parameters of

$$(\rho(x), c(x)) = \begin{cases} \rho_0 = 1000 \text{ kg/m}^3, & c_0 = 1500 \text{ m/s} \quad \text{if } x \leq \alpha \\ \rho_1 = 1200 \text{ kg/m}^3, & c_1 = 2800 \text{ m/s} \quad \text{if } x > \alpha. \end{cases} \tag{61}$$

Numerical experiments are performed on 400 grid points, with CFL $= 0.8$ in medium 1. They are initialized by a spatially bounded right-going wave,

$$U_0(x) = -f_0(\xi)\begin{pmatrix}\frac{1}{c_0}\\ \rho_0\end{pmatrix}. \tag{62}$$

The maximal smoothness is required for the couplage "WENO 5 + ESIM 3-3": in this case, $s = 5$ (56). So, we use a $\mathcal{C}^5$ spatially bounded sinusoidal function $f_0(\xi)$:

$$f_0(\xi) = \begin{cases}\sin(\omega_c\,\xi) - \frac{21}{32}\sin(2\,\omega_c\,\xi) + \frac{63}{768}\sin(4\,\omega_c\,\xi) - \frac{1}{512}\sin(8\,\omega_c\,\xi) & \text{if } 0 < \xi < \frac{1}{f_c},\\ 0 \text{ else,} \quad \text{with } \xi = t_0 - \frac{x}{c}.\end{cases} \tag{63}$$

Left and right values of sixth-order's derivatives of $U_0(x)$ are defined everywhere (as needed in Section 3.4). The central frequency is $f_c = 50$ Hz, and $t_0 = 51$ ms. The initial value of the acoustic pressure, called afterwards the *solution*, is shown in Fig. 3a. After reaching the interface, the acoustic wave is transmitted and reflected. Figures 3b, 3c, and 3d show numerical $(\cdots)$ and exact values (solid line) of the solution at $t = 90$ ms.

Figure 3b shows the solution computed with the couplage "Lax–Wendroff + ESIM 2-2." The dispersive behavior of the Lax–Wendroff scheme is clearly seen in spurious oscillations. Figure 3c shows the solution "TVD + ESIM 2-2." The use of a flux-limiter reduces oscillations but flattens the crests of the wave. Figure 3d shows the solution "WENO 5 + ESIM 3-3." The acoustic wave is very well resolved.

Table I shows the errors in both L_∞ and L_1 norms obtained at $t = 90$ ms with these schemes, with and without the ESIM. Computations are performed in double precision. In

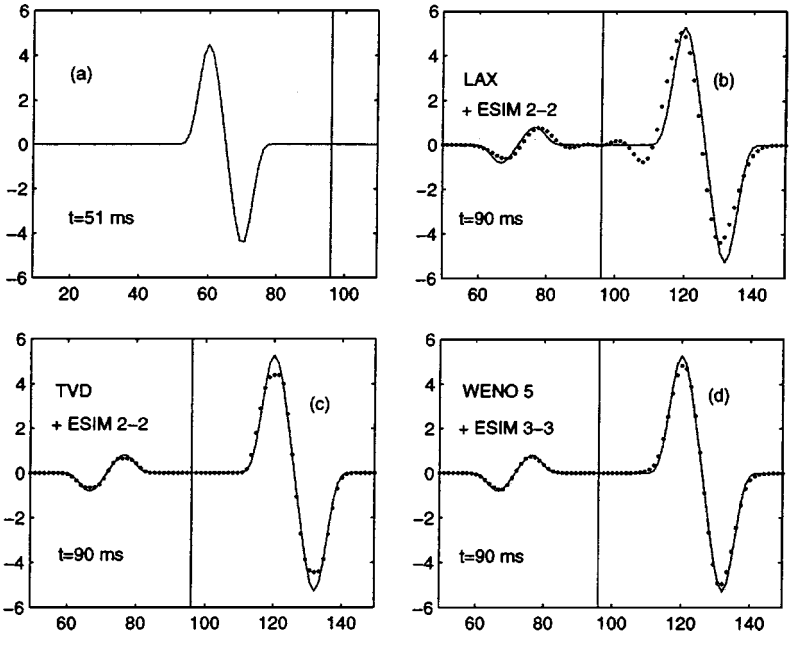

FIG. 3. The exact solution at $t = 51$ ms (a); exact (solid line) and numerical solution $(\cdots)$ at $t = 90$ ms: Lax–Wendroff + ESIM 2-2 (b); TVD + ESIM 2-2 (c); WENO 5 + ESIM 3-3 (d).

TABLE I
Errors and Orders of Accuracy in Section 4.1

Method	N	L_∞ error	L_∞ order	L_1 error	L_1 order
Lax–Wendroff	200	2.38e00	—	8.78e+1	—
	400	8.81e−1	1.43	2.71e+1	1.70
	800	2.15e−1	2.03	7.22e00	1.90
	1600	5.99e−2	1.84	2.06e00	1.81
	3200	3.13e−2	0.93	9.90e−1	1.06
	6400	1.77e−2	0.82	5.73e−1	0.79
Lax–Wendroff	200	2.82e00	—	9.80e+1	—
+ ESIM 2-2	400	1.14e00	1.31	3.20e+1	1.61
	800	3.30e−1	1.78	8.49e00	1.91
	1600	7.80e−2	2.08	2.13e00	1.99
	3200	1.93e−2	2.01	5.33e−1	2.00
	6400	4.82e−3	2.00	1.33e−1	2.00
TVD	200	1.55e00	—	3.86e+1	—
	400	6.03e−1	1.36	1.41e+1	1.45
	800	2.91e−1	1.05	9.47e00	0.57
	1600	1.14e−1	1.34	3.28e00	1.53
	3200	3.48e−2	1.72	1.26e00	1.37
	6400	2.10e−2	0.72	6.94e−1	0.86
TVD	200	1.61e00	—	3.42e+1	—
+ ESIM 2-2	400	6.32e−1	1.35	9.94e00	1.78
	800	2.18e−1	1.53	2.47e00	2.01
	1600	7.35e−2	1.57	6.38e−1	1.95
	3200	2.44e−2	1.59	1.59e−1	2.00
	6400	8.19e−3	1.57	4.05e−2	1.97
WENO 5	200	1.15e00	—	3.29e+1	—
	400	2.20e−1	2.39	6.12e00	2.42
	800	1.30e−1	0.76	4.35e00	0.49
	1600	3.36e−2	1.95	1.05e00	2.04
	3200	4.10e−2	−0.28	9.59e−1	0.14
	6400	1.15e−2	1.83	1.89e−1	2.34
WENO 5	200	7.74e−1	—	2.02e+1	—
+ ESIM 3-3	400	6.13e−2	3.65	1.44e00	3.80
	800	2.96e−3	4.37	8.12e−2	4.15
	1600	1.23e−4	4.58	2.99e−3	4.76
	3200	4.50e−6	4.77	1.03e−4	4.85
	6400	1.55e−7	4.86	3.43e−6	4.90

the case of WENO 5 scheme, the time-step has been adjusted to $\Delta t \sim (\Delta x)^{5/4}$ so that the fourth-order Runge–Kutta in time is effectively fifth-order. When no interface method is used, homogeneized values ρ_i and c_i of ρ and c are used at grid points x_i: ρ_i is the arithmetic average of $\rho(x)$ over $C_i = [x_{i-\frac{1}{2}}, x_{i+\frac{1}{2}}]$, and the bulk modulus K_i is the harmonic average of $K(x)$ over C_i; c_i is deduced by $c_i = \sqrt{K_i/\rho_i}$ [6].

When the ESIM is not used, the order of accuracy is smaller than the theoretical order in homogeneous medium, and it changes a lot with the number of grid points. Using the ESIM (56) and starting at about 400 grid points gives the order of accuracy in a homogeneous medium:

- for Lax–Wendroff, 2 (in both norms),
- for TVD, 1.6 in L_∞ norm and 2 in L_1 norm,
- for WENO 5, tending to 5 (in both norms).

Let us notice that the smoothness of $U_0(x)$ is fundamental to obtain the fifth-order accuracy of the couplage "WENO 5 + ESIM 3-3": only a 3.4 (in L_∞ norm) and 2.4 (in L_1 norm) order is measured for a $\mathcal{C}^2$ function $f_0(\xi)$.

4.2. *Large Contrast Problem: Water–Air Interface*

The previous study is extended to large contrast media. Material properties are

$$\begin{aligned} \rho_0 &= 1000 \text{ kg/m}^3, \quad c_0 = 1450 \text{ m/s} \quad \text{(water)}, \\ \rho_1 &= 1.3 \text{ kg/m}^3, \quad c_1 = 340 \text{ m/s} \quad \text{(air)}. \end{aligned} \tag{64}$$

Differences between exact and numerical values of the solution computed by TVD and WENO 5 schemes with and without interface methods are plotted on Fig. 4. Results are displayed from 20 up to 120 m, at $t = 90$ ms. The scale of the y-axis has been almost amplified by a factor 3 (see y-axis of Fig. 3). Because of the impedance contrast, the wave is almost completely reflected: at this scale, the transmitted wave is not visible. Three subfigures show errors computed with a TVD scheme: without an interface method (a), with the IIM (b), with the ESIM 2-2 (c). Decreasing errors are observed and "WENO 5 + ESIM 3-3" is very accurate (Fig. 4d).

Figure 5 shows errors computed with TVD and WENO 5 schemes in homogeneous water (ρ_0, c_0) at $t = 90$ ms (obviously, no interface method is used). At this time, acoustic waves

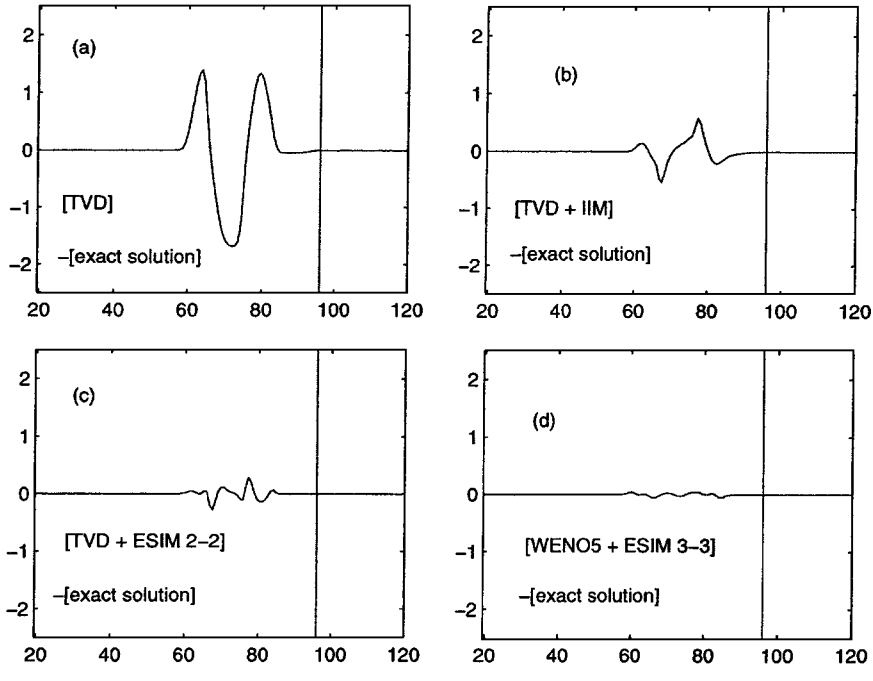

FIG. 4. Differences between numerical and exact values of the solution at $t = 90$ ms (water-air): TVD scheme without an interface method (a); +IIM (b); +ESIM 2-2 (c); WENO 5 + ESIM 3-3, from 20 up to 120 m (d). The vertical line represents the position of the interface.

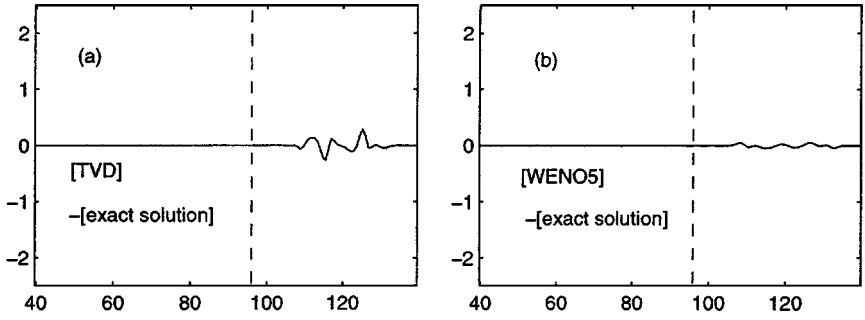

FIG. 5. Differences between numerical and exact values of the solution at $t = 90$ ms (homogeneous water): TVD (a), WENO 5 (b), from 40 up to 140 m. The dotted line recalls the position of the interface water-air in the example of Fig. 4.

have traveled in water the same distance as reflected acoustic waves of Fig. 4. Dotted lines in Fig. 5 recall the position of the interface in Fig. 4.

It is instructive to compare Figs. 4c and 4d, respectively, with Figs. 5a and 5b, after performing symmetries of these last ones in relation to the x-axis and to the dotted vertical line (these symmetries are due to the impedance contrast: $\rho_1 c_1 > \rho_0 c_0$ and to the change in direction). Shapes and levels of errors are then very close. The presence of the interface does not introduce noticeable artefacts when the ESIM is used.

Measures of errors and orders of accuracy have been performed also for various positions of α and values of ϵ (31), confirming the analysis of Section 3.4. If the Lax–Wendroff or TVD scheme is used, and for an interface very close to a grid point ($\epsilon > 0.999$), ESIM 3-2 is used to avoid instabilities (see Section 3.6).

4.3. *2D Plane Wave*

As a last example, we provide a two-dimensional result. The key idea of the ESIM—determination and use of modified values at irregular points—obviously remains the same as in the one-dimensional case. The derivation of jump conditions, the construction of modified values by a least-square resolution, and the analysis of the resulting scheme will be omitted here; the comparaison with other interface methods and the investigation of various cases (interface waves, elastic waves) will also be developed in a future publication. Our goal here is to show only the improvement of the computation when the ESIM is used.

We use an unsplit high-resolution scheme with flux-limiters, called wave-propagation algorithm, developed by Langseth and LeVeque [9, 11]. The acoustic case in a 2D heterogeneous fluid medium is studied in [9].

We consider the case of a plane wave stricking a plane interface that is not aligned with the grid. Exact values of the acoustic pressure (called again the *solution*) of reflected and transmitted waves are easy to determine [1]. The interface is described by

$$\Gamma = \{M(x, y)/y = f(x) = (x - x_0)\tan\theta_0\}, \tag{65}$$

with $\theta_0 = 68^\circ$ and $x_0 = 60.4$ m. Physical parameters are:

$$(\rho(x, y), c(x, y)) = \begin{cases} \rho_0 = 1000 \text{ kg/m}^3, & c_0 = 1500 \text{ m/s} \quad \text{if } y > f(x) \\ \rho_1 = 800 \text{ kg/m}^3, & c_1 = 1000 \text{ m/s} \quad \text{if } y \le f(x). \end{cases} \tag{66}$$

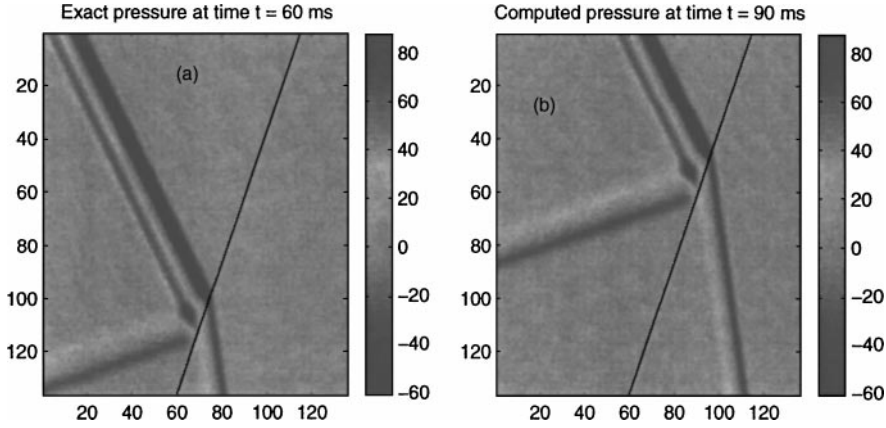

FIG. 6. Plane wave hitting a plane interface that is not aligned with the grid. Exact values of the acoustic pressure at $t = 60$ ms (a) and computed values of the acoustic pressure at $t = 90$ ms (b).

The incident wave is based again on $f_0(\xi)$, with

$$\xi = t_0 - \frac{1}{c_0}(x \cos\theta_i + y \sin\theta_i) \tag{67}$$

where $t_0 = 60$ ms, $\theta_i = 30^\circ$ and $f_c = 50$ Hz. Computations are performed on 136×136 grid points for a 135 m $\times$ 135 m domain, with CFL $= 0.8$ in medium 0 (the wave-propagation algorithm is stable up to CFL $= 1$ in 2D). Because of the stencil, two "ghost cell" lines are defined on each boundary of the domain. Exact values of the acoustic pressure and of acoustic velocities are assigned at ghost cells at each time-step. See [9] for additional remarks.

Figure 6 shows initial values of the solution at $t = 60$ ms, and the computed solution at $t = 90$ ms. Figure 7 shows slices of the exact (solid line) and computed ($\cdots$) reflected and

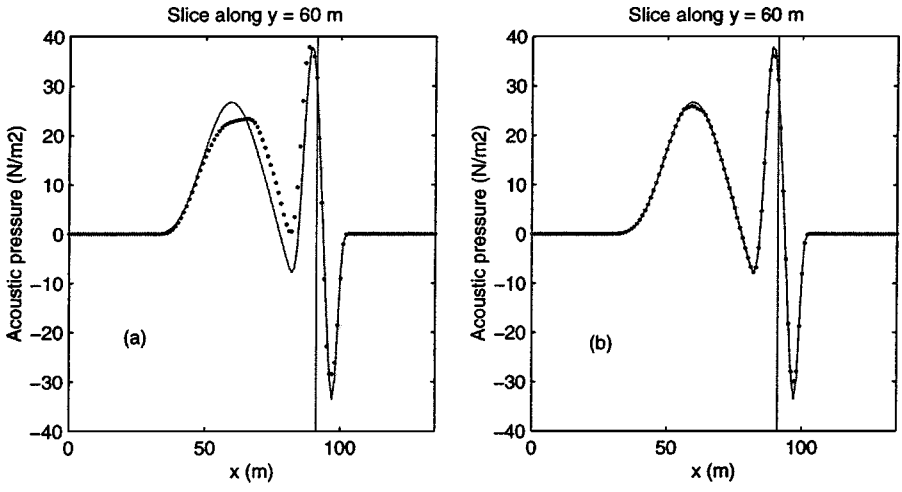

FIG. 7. Plane wave hitting a plane interface that is not aligned with the grid. Values of the acoustic pressure computed by a wave propagation algorithm without an interface method (a) and with the ESIM (b) at $t = 90$ ms, along $y = 60$ m. Exact (solid line) and numerical solution ($\cdots$).

transmitted waves along $y = 60$ m at $t = 90$ ms, without the ESIM (a) and using the ESIM (b). In the first case, we take into account the interface by averaging the physical parameters to obtain values in each grid cell. Then the solution is smeared across the interface. One can find a discussion about this problem in the case of Maxwell equations in [3]. Using an interface method such as the ESIM avoids these numerical artefacts (Fig. 7b).

5. CONCLUSION

A new interface method has been developed and presented in the 1D case, the explicit simplified interface method (ESIM). Modifying *explicitly* numerical values used by a numerical scheme at irregular points amounts to modifying the scheme *implicitly*, so that its order is maintained at irregular points. The implementation of the ESIM can be divided into three independant parts:

- Writing of jump conditions. These conclusions only depend on the physical problem under study and on geometrical features of the interface.
- Construction of modified values during a preprocessing step. This algorithm depends on the scheme's width and order but not on its expression.
- Computation and use of modified values at each time-step.

Qualities of the method have been verified through various numerical examples. The last example (Section 4.4) introduces a future discussion about 2D and 3D applications that we have developed. Interface methods on uniform cartesian grids, such as the ESIM, are of general interest not only for computational acoustics, but also for a wide class of problems such as computational electromagnetics and fluid mechanics.

ACKNOWLEDGMENTS

We thank Jean-Pierre Sessarego (LMA, Marseille) for his confidence and Paul Cristini for introducing us to interface methods. We are grateful to Philippe Angot and Murielle Guichaoua (IRPHEE, Marseille) for numerous suggestions concerning numerical schemes and mathematical background. We thank Arnaud de Ponnat for helpful and very interesting discussions about our method.

REFERENCES

1. L. M. Brekhovskikh, *Waves in Layered Media* (Academic Press, New York, 1980).
2. D. Calhoun, *A Cartesian Grid Method for Solving the Streamfunction Vorticity Equations in Irregular Geometries*, Ph.D. thesis (University of Washington, 1999), available at `ftp://amath.washington.edu/pub/calhoun/thesis/thesis.ps.gz`.
3. F. Collino, P. Joly, and F. Millot, Fictitious domain method for unsteady problems: Application to electromagnetic scattering, *J. Comput. Phys.* **138**, 907 (1997).
4. R. P. Fedkiw, B. Merriman, R. Donat, and S. Osher, *The Penultimate Scheme for Systems of Conservation Laws: Finite Difference ENO with Marquina's Flux Splitting*, Preprint, available at `ftp://ftp.math.ucla.edu/pub/camreport/cam96–18.ps.gz`.
5. T. Fogarty, *High-Resolution Finite Volume Methods for Acoustics in a Rapidly-Varying Heterogeneous Medium*, Master's thesis (University of Washington, 1997), available at `ftp://amath.washington.edu/pub/rjl/students/fogarty:masters.ps.gz`.
6. T. R. Fogarty and R. J. LeVeque, High-resolution finite volume methods for acoustic waves in periodic and random media, *J. Acoust. Soc. Am.* **1**(106), 17 (1999).
7. E. Godlewski and P. A. Raviart, *Numerical Approximation of Hyperbolic Systems of Conservation Laws* (Springer-Verlag, Berlin/New York, 1996).

8. G. S. Jiang and C. W. Shu, Efficient implementation of weighted ENO schemes, *J. Comput. Phys.* **126**, 202 (1996).
9. J. O. Langseth and R. J. LeVeque, A wave-propagation method for three-dimensional hyperbolic conservation laws, *J. Comput. Phys.*, in press, available at `ftp://amath.washington.edu/pub/rjl/papers/jol-rjl:3d.ps.Z`.
10. R. J. LeVeque, *Numerical Methods for Conservation Laws* (Birkhäuser, Basel, 1990).
11. R. J. LeVeque, Wave propagation algorithms for multi-dimensionnal hyperbolic systems, *J. Comput. Phys.* **131**(2), 327 (1997).
12. Z. Li. *The Immersed Interface Method—A Numerical Approach for Partial Differential Equations with Interfaces*, Ph.D. thesis (University of Washington, 1994), available at `ftp://ftp.math.ucla.edu/pub/zhilin/Papers/thesis.ps.Z`.
13. S. I. Rokhlin and Y. J. Wang, Analysis of boundary conditions for elastic wave interaction with an interface betwween two solids, *J. Acoust. Soc. Am.* **89**(2), 503 (1991).
14. A. Wiegmann, *The Explicit Jump Immersed Interface Method and Interface Problems for Differential Equations*, Ph.D. thesis (University of Washington, 1998).
15. C. Zhang, *Immersed Interface Method for Hyperbolic Systems of Partial Differential Equations with Discontinuous Coefficients*, Ph.D. thesis (University of Washington, 1996), available at `ftp://amath.washington.edu/pub/chaoming/dissertation.ps.Z`.
16. C. Zhang and R. J. LeVeque, The immersed interface method for acoustic wave equations with discontinuous coefficients, *Wave Motion* **25**(3), 237 (1997).